Journal of Solid State Chemistry **165,** 48–55 (2002)
doi:10.1006/jssc.2001.9491, available online at http://www/idealibrary.com on IDEAL®

Stability of Rare-Earth Oxychloride Phases: Bond Valence Study

Jorma Hölsä,* Manu Lahtinen,† Mika Lastusaari,*,‡,[1] Jussi Valkonen,† and Jussi Viljanen*

*Department of Chemistry, Laboratory of Inorganic Chemistry, University of Turku, FIN-20014 Turku, Finland; †Department of Chemistry, University of Jyväskylä, P.O. Box 35, FIN-40351 Jyväskylä, Finland; and ‡Graduate School of Materials Research, Turku, Finland
E-mail: miklas@utu.fi

Received July 31, 2001; in revised form November 1, 2001; accepted December 21, 2001

The crystal structures of the tetragonal rare earth (*RE*) oxychlorides, *RE*OCl (*RE* = La–Nd, Sm–Ho, and Y) were studied by X-ray powder diffraction measurements, Rietveld analyses, and bond valence calculations. The tetragonal structure (space group *P*4/*nmm*, No. 129, *Z* = 2) is stable for all but Er–Lu oxychlorides, which possess a hexagonal structure. The tetragonal structure consists of alternating layers of $(REO)_n^{n+}$ complex cations and X^{n-} anions, where the rare earth is coordinated to four oxygens and four plus one chlorines in a monocapped tetragonal antiprism arrangement. The Rietveld analyses yielded a coherent series of structural parameters. Preferred orientation and microabsorption effects were found significant. The evolution of interatomic distances and bond angles indicated that the reason for the preferred structure changing from tetragonal to hexagonal is the strain in the chlorine layer. The bond valence parameter *B* for the *RE*–O bonds had to be recalculated due to the covalent nature of the $(REO)_n^{n+}$ unit. The results obtained with the new parameter confirmed the strains in the chlorine layer to be the cause for the phase transition. © 2002 Elsevier Science (USA)

Key Words: **rare-earth oxychlorides; X-ray powder diffraction; Rietveld analysis; phase transition; bond valence.**

INTRODUCTION

The most efficient and stable commercially used luminescent materials are based on rare earth (*RE*) compounds—or at least on doping with the RE^{3+} (or RE^{2+}) ions (1, 2). *RE* oxycompounds corresponding to the general formula $(REO)_nX$ are amongst these efficient phosphor host lattices. The structural feature typical of all *RE* oxycompounds is a network of alternating layers of $(REO)_n^{n+}$ complex cations and X^{n-} anions (Fig. 1). The $(REO)_n^{n+}$ structural unit is very rigid and stable, which is assumed to be the reason for the efficient luminescence (3), since phase transitions as well as lattice defects usually deteriorate the luminescence.

The crystal structure of lanthanum oxychloride, LaOCl, was first solved in the early 1940s from X-ray powder diffraction patterns as tetragonal (4). This solution has also been confirmed by an X-ray single-crystal study (5). The tetragonal structure has been found stable for all but Er–Lu oxychlorides (ErOCl and YOCl are dimorphic), which possess a hexagonal structure (6). Despite the rather simple structure, the structural data published so far for the tetragonal *RE*OCl (4, 5, 7–14) is incoherent and inconsistent as far as the evolution of the structural parameters is concerned. This inconsistency prevents the systematic use of the structural data as starting information for sophisticated quantum chemical calculations.

The aim of the present work was to produce a coherent structural data set, with the so far lacking TbOCl included. The data are to be used for calculating the optical properties of the oxychlorides including the energy level schemes of the RE^{3+} ions in the extensively studied *RE*OCl matrices (15, 16). The evolution of the magnetic susceptibility as a function of temperature will be simulated, as well (17). The second purpose of this paper is to carry out calculations based on the bond valence model (BVM) to yield information on the stability of the tetragonal *RE*OCl phase and the effects leading to the tetragonal to hexagonal phase transition. Previous BVM calculations (18) have failed because of the incoherency of the structural data.

EXPERIMENTAL

Sample Preparation

The polycrystalline *RE*OCl samples were prepared by a solid state reaction between the freshly prepared *RE* oxide and ammonium chloride in a static nitrogen atmosphere. The oxides were prepared by oxalate precipitation and subsequent firing in air at 1000°C for 3 h to increase the reactivity and ensure similar crystallite size and distribution. However, the Ce, Pr, and Tb oxalates were fired in an ammonia atmosphere to preserve the trivalent state of the

[1]To whom correspondence should be addressed. Fax: +358-2-3336700.

0022-4596/02 $35.00

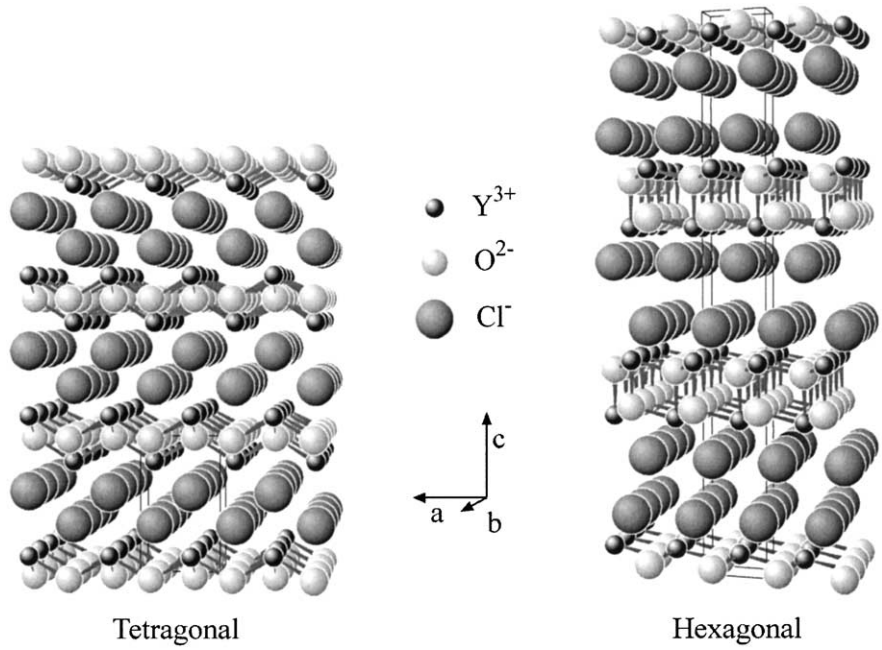

FIG. 1. Layered structures of the tetragonal and hexagonal forms of YOCl.

RE ions. In contrast to the *RE* oxyfluorides (19), no nonstoichiometric *RE*OCl phases exist, which allowed the use of an excess of 5 to 7.5 mol% of ammonium chloride to force the reactions to completeness. The initial mixtures were first heated at 450°C for 0.5 h, and thereafter the temperature was raised to the final one—between 600 and 1000°C (from HoOCl to LaOCl)—for another hour. Pieces of graphite were added into the reactor for the Ce, Pr, and Tb samples to prevent oxidation to RE^{4+}. No measures could, however, be taken to prevent the reduction of Eu^{3+} and Sm^{3+} to Eu^{2+} and Sm^{2+}, whose presence was indicated by magnetic measurements (17). Yttrium and erbium oxychlorides are dimorphic, and thus the yttrium sample was doped with a nominal 1 mol% of trivalent europium to prevent the formation of the hexagonal phase as well to enable eventual luminescence measurements. The purity of the samples was confirmed by routine X-ray powder diffraction measurements.

X-Ray Powder Diffraction

The X-ray powder diffraction patterns of the *RE* oxychlorides were collected with an Enraf-Nonius PDS120 X-ray powder diffractometer equipped with an INEL CPS120 position sensitive detector. The measurements were carried out at room temperature between 5° and 125° in 2θ by using copper $K\alpha_1$ radiation ($\lambda = 1.54060$ Å) and a flat rotating sample holder. The data collecting time was 90 min. A mixture of silicon (NIST standard 640b) and fluorophlogopite (NIST standard 675) powders was used as an external standard. The angular resolution of the apparatus was better than 0.018° in θ.

Rietveld Analysis

The X-ray powder diffraction data were analyzed with the Rietveld profile refinement method (20) by using the FullProf program (21). The analyses were performed in the 2θ range from 20° to 110°. In the refinements, the parameters were turned on in the following sequence: zero point for 2θ, background (a fifth-order polynomial function), scale factor, unit cell parameters a and c, fractional atomic coordinates, half-width parameters U, V, and W, peak asymmetry parameter, profile shape parameter, and isotropic temperature factors B. The peak asymmetry correction was accounted for in the whole 2θ range. Pseudo-Voigt profile form function was used, and Bragg–Brentano geometry was assumed. Because the preliminary refinements gave clear evidence of the phenomena, corrections for preferred orientation (Rietveld model) and microabsorption were applied. Since the plate-like crystallites were expected to orientate in such a way that the unit cell c axes are parallel to each other, the preferred orientation vector was given as (0, 0, 1).

Bond Valence Model

The dependence of the bond length on the coordination number of a cation was first discovered by Goldschmidt while studying metallic compounds in the late 1920s (22).

Pauling introduced the electrostatic bond strength or bond valence (BV) for ionic crystals, stating that the bond valence is obtained by dividing the charge of an ion by its coordination number of (23). The sum of the bond valences of a given ion gives its charge (Pauling's second rule).

The most commonly used semiempirical relationships between the bond valence (s_{ij}) and the bond length are (24)

$$s_{ij} = (R_{ij}/R_0)^{-N} \quad [1]$$

$$s_{ij} = \exp((R_0 - R_{ij})/B), \quad [2]$$

where R_{ij} is the experimental bond length, R_0 the characteristic length (25), and N and B are empirical parameters. In this work, Eq. [2] proposed by Zachariasen (26) is used.

Zachariasen (26) reported BV parameter values for the bonds between oxygen or halides (X) and the 3d, 4d, 5d–5f, and 6d–5f elements with B values from 0.314 to 0.35 Å for the M–O bonds and 0.40 for the M–X bonds. Later, Brown and Altermatt (27) reported a set of R_0 values determined from 750 atom pairs and stated that the B parameter value of 0.37 Å is valid for most bonds and can be considered universal. Brese and O'Keeffe (25) assumed the universal value and reported a more complete set of R_0 values derived from well over 1000 crystal structures. On the other hand, the universal applicability of the B value equal to 0.37 Å and the R_0 values determined by using it have been contested for, e.g., Mo–O (24), Pb–O (28), and bonds in anion-centered metal tetrahedra (29) and alkali halides and chalcogenides (30) in general. However, modifying both R_0 and B is rather dubious and may lead to the loss of both physical and chemical information. R_0 and B may simply become fitting parameters, destroying the general applicability of the BVM.

The BVM has been used in modeling crystal structures (31) as well as to predict bonding topologies (32), bond lengths (33), and even complete crystal structures (34). Missing atoms can be located by calculating valence-sum maps when carrying out crystal structure determinations (35), and information on the site occupancies in solid solutions may be obtained (36). The correctness of structural solutions can be tested (37) as well as the stabilities of compounds evaluated (35). The BVM has been used in a study of ion transport in fast ion-conducting glasses together with reverse Monte Carlo modeling (38). Effective atomic valences can help distinguish between oxidation states of metals (37) and give information on electron conduction paths (39). Also, the BVM was the basis for obtaining the charge factors for the simple overlap model used for calculating the crystal field effect from structural data (40).

One derivative of the bond valence model (BVM) is the global instability index (GII) value,

$$\mathrm{GII} = \sqrt{\sum_{i=1}^{N} \left(\frac{\sum_j (s_{ij} - V_i)^2}{N} \right)}, \quad [3]$$

which can be used to estimate the stability of a compound. This quantity is defined by a comparison between the calculated bond valences and the formal valence (V_i) for all the species (N) in the asymmetric unit (41).

BV calculations can also give information on the covalent or ionic character of a bond. According to Brown and Shannon (36) the covalency of (f_c') of a bond is given as

$$f_c' = a s_{ij}^M, \quad [4]$$

where a and M are constants, whose values are dependent on the number of core electrons of the cation. For the rare earths, a and M are equal to 0.49 and 1.57, respectively. The covalent character of the bond can be calculated from f_c'/s_{ij}. This quantity has been used to characterize the nature of different O–H bonds in crystals (36).

RESULTS AND DISCUSSION

Diffraction Data

The X-ray powder diffraction patterns show no significant changes between the individual *RE*OCl samples (Fig. 2). The reflection positions move smoothly from the lower 2θ angles toward the higher ones as the *RE* ionic radius decreases. No indication of the symmetry being

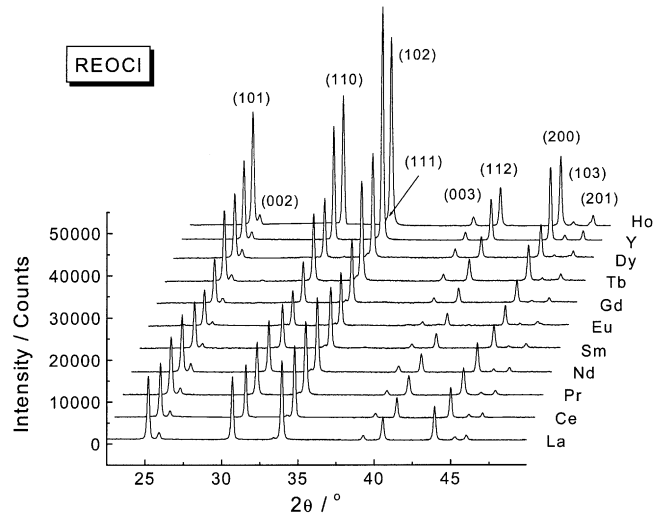

FIG. 2. Room temperature X-ray power diffraction patterns of tetragonal *RE*OCl.

lower than tetragonal could be observed. The observed intensities follow the trend set by the Cu$K\alpha$ mass attenuation coefficients of the individual *RE* elements (42) indicating a rather consistent sample quality throughout the whole *RE*OCl series. The patterns indicate that the Ce, Eu, Dy, and Ho samples contained traces of oxide impurities, which were left out from the Rietveld refinements as excluded regions. Furthermore, magnetic measurements (17) suggested that in addition to the trivalent *RE* ions both the EuOCl and SmOCl samples contained some divalent cations, as well. All the samples seem to crystallize in the tetragonal Matlockite (PbFCl)-type structure, and due to the 1 mol% Eu^{3+} doping, the dimorphic YOCl showed no traces of the hexagonal SmSI-type form.

Rietveld Analyses

The PbFCl-type structure crystallizes in the tetragonal $P4/nmm$ space group, $Z = 2$, with the RE^{3+} ion coordinated to four oxide and to four plus one chloride ions in a monocapped square antiprism arrangement. The RE^{3+} and the chloride ions occupy the 2c $(\frac{1}{4}, \frac{1}{4}, z)$ and the oxide ions the 2a $(\frac{1}{4}, \frac{3}{4}, 0)$ positions with C_{4v} and D_{2d} site symmetries, respectively.

The simulations yielded good fits between the experimental and calculated patterns (Fig. 3). This is indicated by the satisfactory Bragg *R* values (Table 1). The Bragg *R* can usually be considered the *R* value that gives the most reliable picture of the actual goodness of the fit, even if the choice of profile function may have a strong effect on its value (43). The R_{wp} values decrease with increasing background as expected (43). The χ^2 parameter never reached its ideal value of 1, since with a data collecting time of 90 min the counting statistics errors are much less significant than those between the actual structure and the structural model. The χ^2 values thus indicate that the estimated standard deviation (esd) values of the structural parameters obtained from the refinements are underestimated.

The unit cell *a*- and *c*-axis lengths as well as the unit cell volumes of the *RE* oxychlorides decrease linearly ($R_a = 0.998$, $R_c = 0.999$, and $R_V = 0.998$) as the ionic radius of the RE^{3+} host cation decreases (Fig. 4). When compared with the change of the RE^{3+} ionic radius the *c*-axis length decreases faster than the *a*-axis one, and a linear fit of the experimental points (with the same *R* values as those given above) shows that the *a*-axis change is 1.5 times and the *c*-axis 1.9 times that of the ionic radius. The esd values of the cell parameter *a* and *c* values obtained from the refinements were 2×10^{-5} for *a* and 3×10^{-5} Å for *c*. The experimentally observed precision for the *a* parameter with the current experimental setup and crystal structure is 10^{-3} Å, thus making those calculated underestimated by up to a factor of 50.

The *z* coordinate of the RE^{3+} ion position decreases rather linearly from LaOCl to HoOCl, while *z*(Cl) changes much less and achieves a maximum at EuOCl (Fig. 5). These results were obtained by using the microabsorption and preferred orientation corrections. The *RE z*-coordinate values are unaffected by the corrections, but the uncorrected *z*(Cl) values for EuOCl, GdOCl, TbOCl, and HoOCl were too different from the trend set by the other *RE*OCl. The conventional wisdom tells that the evolution should be smooth for an isostructural series such as the *RE* oxychlorides. A detailed study of the effect of preferred orientation and microabsorption correction will be published elsewhere.

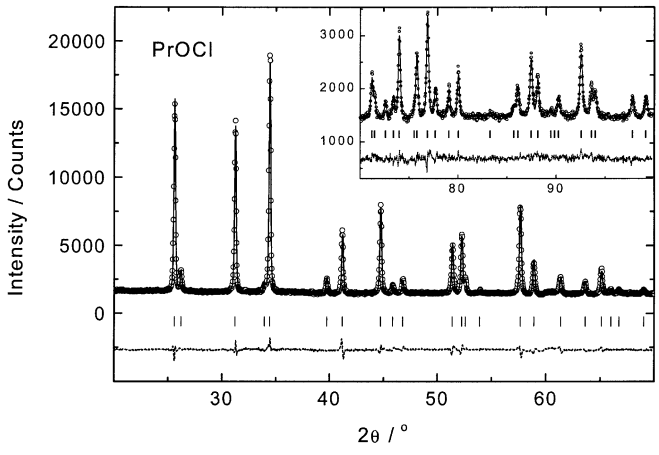

FIG. 3. Rietveld plot of the tetragonal PrOCl at room temperature. The circles show the observed pattern, the solid line shows the calculated pattern, the dashed line shows the difference, and the bars show the Bragg reflections

Trends in Crystal Structure

The *RE*–O ($\times 4$), *RE*–Cl ($\times 4$), and *RE*–Cl ($\times 1$) distances decrease linearly as a function of the RE^{3+} ionic radius (Fig. 6, Table 2) with the linear fits giving *R* values of 0.999, 0.996, and 0.990, respectively. The *RE*–O distances are about 10% shorter than the sum of the respective ionic radii (44), indicating that the bonding is clearly of covalent nature. The *RE*–Cl bond lengths, all somewhat larger than the sum of the ionic radii (44), get closer to each other as the RE^{3+} ionic radius decreases, thus giving the compounds a more ionic character. For the smaller *RE*s, the difference between *RE*–Cl ($\times 4$) and *RE*–Cl ($\times 1$) bond lengths appears to become constant. It seems that for the *RE*s smaller than holmium the hexagonal form is the preferred one, because maintaining the difference of the two *RE*–Cl distances, or even decreasing it, would bring the chlorines too close to one another. Usually, the ionic radius of Cl^- is considered to be 1.81 Å (44), which, not

TABLE 1
Rietveld Refinement Results for the Tetragonal *RE*OCl

*RE*OCl	a (Å)	c (Å)	V(Å^3)	z(*RE*)	z(Cl)	B(*RE*) (Å^2)	B(O) (Å^2)	B(Cl) (Å^2)	R_B(%)	R_{wp}(%)	χ^2	GII/v.u.
LaOCl	4.11679(1)	6.87450(2)	116.51	0.1750(1)	0.6290(5)	0.78(3)	0.96(21)	1.22(8)	5.1	5.1	3.3	0.089
CeOCl	4.07491(1)	6.83434(2)	113.48	0.1741(2)	0.6294(6)	0.66(2)	0.90(27)	1.13(10)	5.5	5.2	4.1	0.093
PrOCl	4.04796(1)	6.79760(2)	111.39	0.1734(2)	0.6298(6)	0.83(2)	0.40(22)	1.22(9)	6.2	3.7	2.4	0.097
NdOCl	4.02013(1)	6.76547(2)	109.34	0.1733(2)	0.6298(7)	0.76(4)	0.26(26)	1.25(11)	7.3	3.8	3.0	0.085
SmOCl	3.97860(1)	6.71638(3)	106.32	0.1712(3)	0.6303(9)	0.82(6)	0.27(32)	1.37(15)	9.7	3.0	2.5	0.090
EuOCl	3.95958(2)	6.68703(3)	104.84	0.1712(4)	0.6300(13)	1.48(7)	1.99(53)	1.76(20)	12.6	3.4	3.5	0.084
GdOCl	3.94631(1)	6.66099(3)	103.73	0.1707(3)	0.6310(10)	1.29(7)	0.32(33)	1.92(16)	9.5	2.8	2.5	0.081
TbOCl	3.92443(1)	6.64188(3)	102.29	0.1701(2)	0.6299(8)	0.86(4)	0.61(26)	1.33(11)	6.2	2.9	2.9	0.088
DyOCl	3.90763(1)	6.61477(3)	101.00	0.1691(2)	0.6294(9)	0.91(6)	0.64(31)	1.37(14)	6.3	3.1	3.6	0.102
YOCl	3.90010(1)	6.59339(2)	100.29	0.1666(2)	0.6289(5)	0.82(4)	0.73(18)	1.43(7)	8.6	13.1	15.9	0.135
HoOCl	3.89037(1)	6.59514(2)	99.82	0.1685(2)	0.6281(6)	1.53(4)	0.68(23)	1.01(9)	4.2	10.6	14.0	0.103

considering electrostatic repulsion, indicates that the minimum distance between two chlorides is 3.62 Å. The shortest Cl–Cl distance in LaOCl is 3.41 Å (decreasing linearly to 3.25 Å for HoOCl), which suggests the presence of considerable strains in the chloride layer. This assumption is further confirmed when comparing the shortest Cl–Cl distances to the 3.72 Å of the SmSI-type YbOCl (6), where the Cl–Cl repulsion seems to be relaxed. The shortest Cl–Cl distance in the PbFCl type is that between the chlorines on the square plane. If the structural change was only due to the repulsion between the chlorines, the same change should be observed for the oxybromides and iodides, as well. The *RE* oxyiodide series is, however, isomorphous, while LuOBr (45) can crystallize with the hexagonal structure. In the *RE*OBr series the strains are allowed to relax along the unit cell c axis, since the c-axis length increases with decreasing RE^{3+} ionic radius (46), but this appears not to be the case with the oxychlorides. The chloride ions are probably not small enough to form only the hexagonal structure (like the *RE* oxyfluorides) or large enough to form only the tetragonal structure (like the *RE* oxybromides and -iodides). It seems that with a sufficiently small RE^{3+} ionic radius, there is enough space for the chloride ions to rearrange and thereby relax the strains present in the tetragonal form. As a result, the $(REO)^{+}$ unit also rearranges, yielding the hexagonal structure, even if the O–O distances in the tetragonal form (from 2.91 to 2.76 Å from LaOCl to HoOCl, respectively) are never shorter than the sum of two O^{2-} ionic radii (2.76 Å (44)). The hexagonal form has less strained chloride layers as a result of a looser packing along the unit cell axis, while a more efficient packing is achieved in the *ab* plane as the RE^{3+} coordination polyhedron changes to the distorted bicapped trigonal antiprism (Fig. 1).

The Cl–*RE*–Cl bond angle with the chlorines located on the opposite corners of the square plane changes clearly more than the O–*RE*–O one as a function of the RE^{3+} ionic radius (Fig. 7, Table 2). The O–*RE*–O angle stays

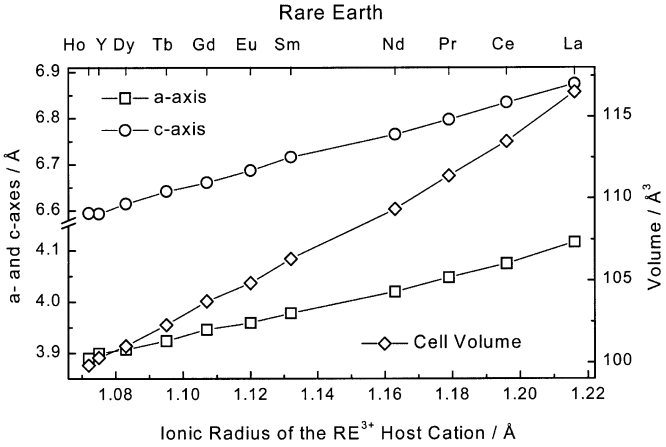

FIG. 4. Evolution of the unit cell axis lengths and volume in the tetragonal *RE*OCl series. The esd values are smaller than the symbol heights.

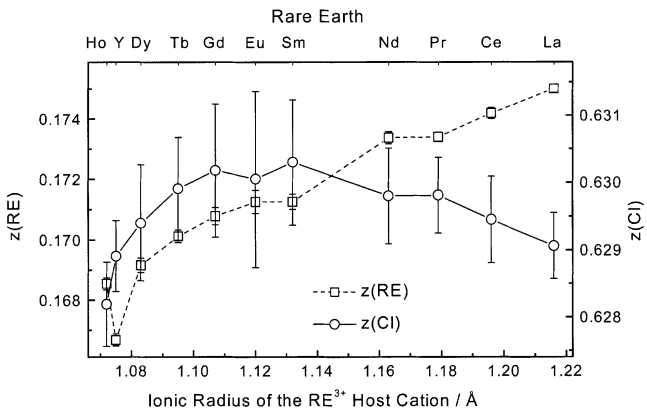

FIG. 5. Evolution of the rare earth and chloride position z coordinates in the tetragonal *RE*OCl series. The error bars give the calculated esd values. Note that the scales of the two plots are different.

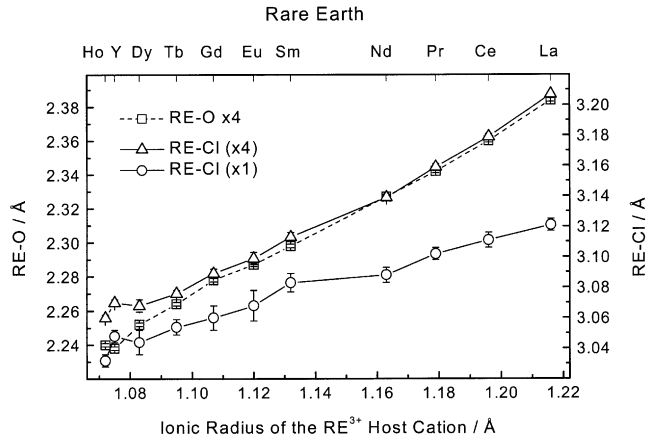

FIG. 6. Evolution of the bond lengths in the tetragonal *RE*OCl. The error bars give the calculated esd values.

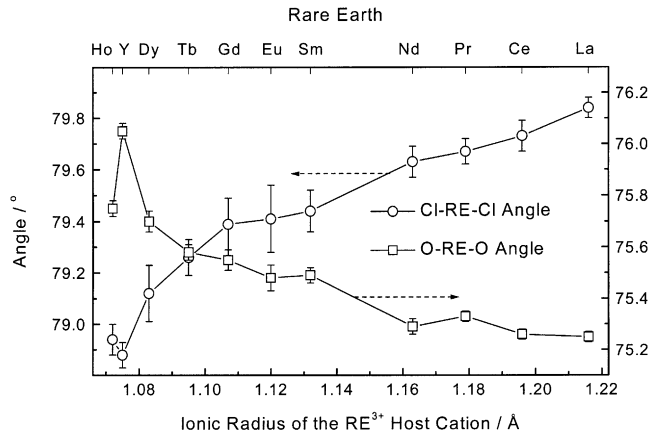

FIG. 7. Evolution of the Cl–*RE*–Cl and O–*RE*–O bond angles. The error bars give the calculated esd values.

nearly constant from LaOCl to NdOCl and thereafter starts increasing, whereas the Cl–*RE*–Cl angle shows a slow decrease from LaOCl to PrOCl, then achieves an almost constant value, and finally decreases quite rapidly starting from TbOCl. This fast decrease further confirms the assumption that the preferred structure changes from tetragonal to hexagonal at the end of the *RE*OCl series, because the chloride layer is allowed to rearrange.

Bond Valence Calculations

The global instability index describes the strains in a structure and puts a limit to the maximum distortion allowed. According to an empirical formulation, with the GII values exceeding 0.2 the structure becomes unstable and faces a possible collapse or a phase transformation (41). In the *RE*OCl series the strains should increase with decreasing RE^{3+} ionic radius, but the GII value decreases if calculated by using the tabulated R_0 values (25) and the universal value 0.37 Å for the B parameter. Clearly, the effect of the structure becoming more ionic, as calculated by Eq. [4] (Fig. 8), resulting from the chloride layer becoming more compact, outweighs that of the strains in the chloride layer. The oxide ions contribute much more than the RE^{3+} ions or the chlorides to the GII value, even if the $(RE\mathrm{O})^{+}$ unit is the most stable part of the *RE* oxychlorides with strong bonding that can be broken only at temperatures higher than 6000 K (47). Moreover, the *RE*–O distances are still longer than those in the very stable $(RE\mathrm{O})^{+}$ unit of the hexagonal *RE* oxides (e.g., 2.384 Å in LaOCl and 2.365 Å in La_2O_3 (48)), which can be obtained by heating the oxychlorides in air. The contribution of the oxygen atoms to the GII value therefore cannot be large due to strains, but because the bonds in the $(RE\mathrm{O})^{+}$ unit are of covalent nature and hence are shorter than the ionic bonds that the BV parameter values used have been derived from.

The BVM should be applicable for both ionic and covalent structures, since the physical nature of the bonds is not implied in its definition. Therefore, the validity of the

TABLE 2
Selected Interatomic Distances and Bond Angles in Tetragonal *RE*OCl

*RE*OCl	*RE*–O × 4 (Å)	*RE*–Cl × 4 (Å)	*RE*–Cl × 1 (Å)	O–*RE*–O (°)	Cl–*RE*–Cl (°)
LaOCl	2.384(1)	3.207(1)	3.121(4)	75.25(2)	79.84(4)
CeOCl	2.360(1)	3.179(2)	3.111(5)	75.26(2)	79.73(6)
PrOCl	2.342(1)	3.159(2)	3.102(4)	75.33(2)	79.67(5)
NdOCl	2.327(1)	3.139(2)	3.088(5)	75.29(3)	79.63(6)
SmOCl	2.298(1)	3.113(3)	3.083(6)	75.49(3)	79.44(8)
EuOCl	2.287(1)	3.099(4)	3.068(10)	75.48(5)	79.41(13)
GdOCl	2.278(1)	3.089(3)	3.060(8)	75.55(4)	79.39(10)
TbOCl	2.264(1)	3.076(2)	3.054(5)	75.58(3)	79.26(7)
DyOCl	2.252(1)	3.068(4)	3.044(8)	75.70(4)	79.12(11)
YOCl	2.238(1)	3.070(2)	3.048(4)	76.05(3)	78.88(5)
HoOCl	2.240(1)	3.060(2)	3.032(4)	75.75(3)	78.94(6)

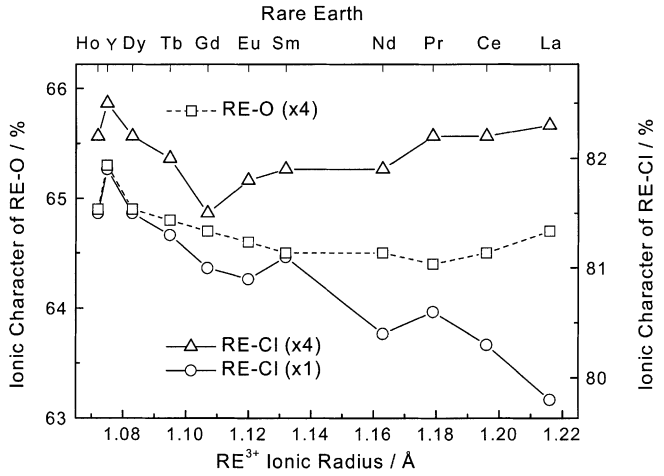

FIG. 8. Ionic character of the *RE*–O and *RE*–Cl bonds of the *RE* oxychlorides calculated with the universal bond softness parameter *B* value 0.37 Å.

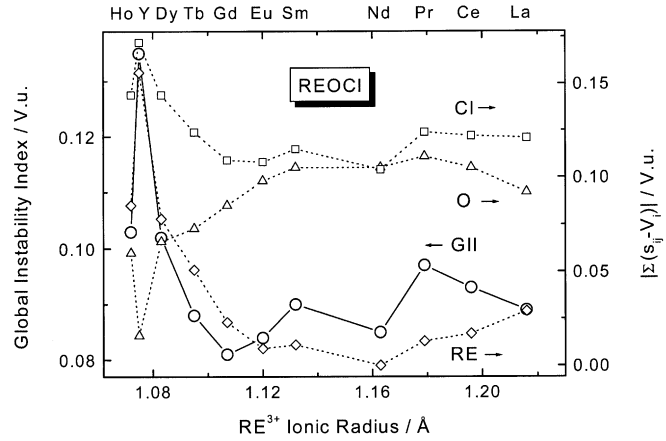

FIG. 9. Global instability index GII values and the contribution of the individual ions to the GII value in the *RE* oxychlorides. The values were calculated by using the corrected bond softness parameter *B* obtained from *RE* oxycompounds.

values of the parameters R_0 and B must be considered. The structural data available for La oxycompounds (13 compounds) containing the $(REO)_n^{n+}$ unit (4, 5, 48–58) revealed that the weighted mean La–O distance within the $(REO)_n^{n+}$ unit is 2.399 Å (ranging from 2.365 to 2.455 Å). This distance was used to optimize the B parameter value by keeping the R_0 constant with the value 2.172 Å given by Brese and O'Keeffe (25) and requiring that the bond valence sum around the oxygen be equal to 2.0 v.u. The resulting B parameter value for the La–O bonds in the $(LaO)_n^{n+}$ unit was 0.33 Å, which according to Urusov (59) applies to many cation–oxygen bonds. Due to the chemical similarity of the *RE*s it can be assumed that this value is applicable for the whole series (except maybe for yttrium). Since only the B parameter should be affected by the nature of the bond, no reason was found for calculating new values for the R_0 parameters, as well. Moreover, the bonding between the *RE* and the chlorides is ionic and thus there is no physical justification for recalculating the R_0 and/or B for the *RE*–Cl bonds.

The GII values were recalculated by using the universal B value of 0.37 Å for the ionic *RE*–Cl bonds and the 0.33 Å value for the covalent *RE*–O bonds. Even if the evolution is not completely smooth, the new GII values decrease slowly from LaOCl to EuOCl and thereafter increase rather sharply, predicting the tetragonal to hexagonal phase transition (Fig. 9). Moreover, the GII of YOCl is clearly the largest, indicating its dimorphic nature. Also, the contributions of the different ions to the GII value (Fig. 9) show that the chloride has the largest effect. The bond valence sum around the chloride increases from GdOCl to HoOCl as an indication of a growing preference for a rearrangement of the chloride layer; i.e., the strain in the chloride layer is the main contributor to the phase transition. This is in agreement with that suggested by the interatomic distances and bond angles.

CONCLUSIONS

Rietveld analyses of the room temperature X-ray powder diffraction patterns of the tetragonal *RE* (*RE* = La–Nd, Sm–Ho, and Y) oxychlorides yielded a coherent series of structural parameters. An ordinary laboratory X-ray setup was thus found sufficient for exact and consistent structural data. Preferred orientation and microabsorption effects were observed to be significant. This indicated that even if the sample-based effects may be of little significance when the structure of an individual compound is determined, they cannot be neglected when a series of isostructural compounds is studied. These effects were accounted for by applying the respective corrections during the Rietveld analyses.

The evolution of the interatomic distances and bond angles indicated that the reason for the most stable structure changing from the tetragonal PbFCl type to the hexagonal SmSI type starting from ErOCl is the strain in the chlorine layer. Once the RE^{3+} ion is small enough, the strains are allowed to relax via a rearrangement of the chlorine layer, which is thereafter followed by a rearrangement of the $(REO)^{+}$ unit, as well.

The global instability index GII values based on the universal bond softness parameter B for the *RE*–O bonds may not be used for the *RE* oxychlorides containing the rigid $(REO)_n^{n+}$ unit, since the parameter has been derived from more ionic structures. In fact, the GII values obtained were observed to be much more influenced by the ionicity of the compound than by the structural strains. Redetermining the bond softness parameter from the bond lengths

of different *RE* oxycompounds resulted in GII values, which predicted the tetragonal to hexagonal phase transition and shows that the transition results from the strains in the chloride layer.

ACKNOWLEDGMENTS

Financial support from the University of Turku, the Academy of Finland as well as from the Graduate School of Materials Research (Turku, Finland) is gratefully acknowledged.

REFERENCES

1. S. Shionoya and W. Yen (Eds.), "Phosphor Handbook." CRC Press, Boca Raton, FL, 1999.
2. G. Blasse and B. C. Grabmaier, "Luminescent Materials." Springer-Verlag, Berlin, 1994.
3. P. Porcher and P. Caro, *J. Less-Common Met.* **93,** 151 (1983).
4. L. G. Sillén and A.-L. Nylander, *Svensk Kem. Tidskr.* **53,** 367 (1941).
5. L. H. Brixner and E. P. Moore, *Acta Crystallogr. Sect. C* **39,** 1316 (1983).
6. G. Brandt and R. Diehl, *Mater. Res. Bull.* **9,** 411 (1974).
7. E. Garcia, J. D. Corbett, J. E. Ford, and W. J. Vary, *Inorg. Chem.* **24,** 494 (1985).
8. D. H. Templeton and C. H. Dauben, *J. Am. Chem. Soc.* **75,** 6069 (1953).
9. H. P. Beck, *Z. Naturforsch. b* **32,** 1015 (1977).
10. W. H. Zachariasen, *Acta Crystallogr.* **2,** 388 (1949).
11. M. Wolcyrz and L. Kepinski, *J. Solid State Chem.* **99,** 409 (1992).
12. G. Meyer and T. Schleid, *Z. Anorg. Allg. Chem.* **533,** 181 (1986).
13. H. Bärnighausen, G. Brauer, and N. Schultz, *Z. Anorg, Allg. Chem.* **338,** 250 (1965).
14. J. Aride, J. P. Chaminade, and M. Pouchard, *J. Cryst. Growth* **57,** 194 (1982).
15. R.-J. Lamminmäki, Ph.D. Thesis. University of Turku, Turku, Finland, 1999.
16. J. Hölsä and R.-J. Lamminmäki, *J. Lumin.* **69,** 311 (1996).
17. J. Hölsä and R.-J. Lamminmäki, M. Lastusaari, P. Porcher, and R. Sáez-Puche, *J. Alloys Compd.* **303–304,** 498 (2000).
18. J. Hölsä, K. Koski, R.-J. Lamminmäki, H. Rahiala, and E. Säilynoja, *Acta Phys. Pol.* **91,** 563 (1997).
19. J. Hölsä, E. Säilynoja, H. Rahiala, and J. Valkonen, *Polyhedron* **16,** 3421 (1997).
20. H. M. Rietveld, *J. Appl. Cryst.* **2,** 65 (1969).
21. J. Rodriguez-Carvajal, "FullProf version 3.2 Jan/97." Laboratoire Leon Brillouin (CEA-CNRS), Gif sur Yvette, France 1997, unpublished.
22. V. M. Goldschmidt, *Z. Phys. Chem.* **133,** 397 (1928).
23. L. Pauling, *J. Am. Chem. Soc.* **51,** 1010 (1929).
24. F. Zocchi, *Solid State Sci.* **2,** 383 (2000).
25. N. E. Brese and M. O'Keeffe, *Acta Crystallogr. Sect. B* **47,** 192 (1991).
26. W. H. Zachariasen, *J. Less-Common Met.* **62,** 1 (1978).
27. I. D. Brown and D. Altermatt, *Acta Crystallogr. Sect. B* **41,** 244 (1985).
28. S. V. Krivovichev and I. D. Brown, *Z. Kristallogr.* **216,** 245 (2001).
29. S. V. Krivovichev, *Z. Kristallogr.* **214,** 371 (1999).
30. S. Adams, *Acta Crystallogr. Sect. B* **57,** 278 (2001).
31. I. D. Brown, *Z. Kristallogr.* **199,** 255 (1992).
32. V. S. Urusov, *Z. Kristallogr.* **216,** 10 (2001).
33. B. A. Hunter, C. J. Howard, and D.-J. Kim, *J. Solid State Chem.* **146,** 363 (1999).
34. A. Santoro, I. Natali Sora and Q. Huang, *J. Solid State Chem.* **143,** 69 (1999).
35. I. D. Brown, *Acta Crystallogr. Sect. B* **48,** 553 (1992).
36. I. D. Brown and R. D. Shannon, *Acta Crystallogr. Sect. A* **29,** 266 (1973).
37. A. Santoro, I. Natali Sora, and Q. Huang, *J. Solid State Chem.* **151,** 245 (2000).
38. J. Swenson and S. Adams, *Phys. Rew. B* **64,** 024204 (2001).
39. F. Liebau, *Z. Kristallogr.* **215,** 381 (2000).
40. R. Q. Albuquerque, G. B. Rocha, O. L. Malta, and P. Porcher, *Chem. Phys. Lett.* **331,** 519 (2000).
41. A. Salinas-Sanchez, J. L. Garcia-Muñoz, J. Rodriguez-Carvajal, R. Sáez-Puche, and J. L. Martinez, *J. Solid State Chem.* **100,** 201 (1992).
42. K. Lonsdale (Ed.), "International Tables for X-ray Crystallography, Vol. 3. Physical and Chemical Tables," p. 163. Kynoch, Birmingham, UK, 1962.
43. J. Hölsä, M. Lastusaari, and J. Valkonen, *Mater. Sci. Forum.* **278–281,** 38 (1998).
44. R. D. Shannon, *Acta Crystallogr. Sect. A* **32,** 751 (1976).
45. M. B. Novikova, B. A. Popovkin, L. N. Cholodkoskaja, and V. M. Skorikov, *Vestn. Mosk. Un-ta. Ser. 2 Chimija* **30,** 467 (1989).
46. J. Hölsä, M. Lahtinen, M. Lastusaari, J. Niittykoski, and J. Valkonen, *in* "19th Eur. Cryst. Meeting" Nancy France, Aug. 25–31, 2000, p. 350.
47. E. Antic and P. Caro, *Spectrochim. Acta B* **27,** 479 (1972).
48. P. Aldebert and J. P. Traverse, *Mater. Res. Bull.* **14,** 303 (1979).
49. J. Hölsä, M. Lastusaari, and J. Valkonen, *J. Alloys Compd.* **262–263,** 299 (1997).
50. B. Morosin and D. J. Newman, *Acta Crystallogr. Sect. B* **29,** 2647 (1973).
51. Y. Hashimoto, M. Takahashi, S. Kikkawa, and F. Kanamaru, *J. Solid State Chem.* **114,** 592 (1995).
52. S. Zhukov, A. Yatsenko, V. Chernyshev, V. Trunov, E. Tserkovnaya, O. Antson, J. Hölsä, P. Baulés, and H. Schenk, *Mater. Res. Bull.* **32,** 43 (1997).
53. J. S. Xue, M. R. Antonio, and L. Soderholm, *Chem. Mater.* **7,** 333 (1995).
54. J. Hölsä, M. Lahtinen, M. Lastusaari, and J. Valkonen, unpublished (1998).
55. E. Gobichon, J.-P. Auffrédic, and D. Louër, *Solid State Ionics* **93,** 51 (1997).
56. J. Ostoréro and M. Leblanc, *Acta Crystallogr. Sect. C* **46,** 1376 (1990).
57. P. M. Raccah, J. M. Longo, and H. A. Eick, *Inorg. Chem.* **6,** 1471 (1967).
58. R. L. Seiver and H. A. Eick, *J. Less-Common Met.* **44,** 1 (1976).
59. V. S. Urusov, *Acta Crystallogr. Sect. B* **51,** 641 (1995).